Obstructed Breakup of Slender Drops in a Microfluidic *T* Junction

A. M. Leshansky,[1,*] S. Afkhami,[2] M.-C. Jullien,[3] and P. Tabeling[3]

[1]*Department of Chemical Engineering, Technion-IIT, Haifa, 32000, Israel*

[2]*Department of Mathematical Sciences, New Jersey Institute of Technology, Newark, New Jersey 07102, USA*

[3]*MMN, CNRS, ESPCI Paris-Tech, 10 rue Vauquelin, 75005 Paris, France*

(Received 12 February 2012; published 26 June 2012)

In this Letter we present a theoretical analysis of the droplet breakup with "permanent obstruction" in a microfluidic *T* junction [M.-C. Jullien *et al.*, Phys. Fluids **21**, 072001 (2009)]. The proposed theory is based on a simple geometric construction for the interface shape combined with Tanner's law for the local contact angle. The resulting scaling of the droplet deformation with time and capillary number is in excellent agreement with the results of direct numerical simulations and prior experiments. More rigorous analysis based on the lubrication approximation reveals a self-similar behavior analogous to the classical problem of a droplet spreading over a preexisting liquid film.

DOI: 10.1103/PhysRevLett.108.264502 PACS numbers: 47.55.D−, 47.55.N−, 47.61.Jd, 68.03.Cd

Digital or droplet-based microfluidics is a fast developing interdisciplinary field of research combining soft matter physics, biochemistry and microsystems engineering [1]. The use of droplets as "micro reactors" offers many advantages in comparison with single-phase microfluidics such as confinement of reactants or prevention of axial dispersion and cross talk between different samples, reduction of unwanted adhesion (adsorption) of the substances confined in droplets at the channel walls, facilitated heat (mass) transport due to enhanced internal mixing, and others. Various techniques have been proposed and tested for production and manipulation of droplets in microfluidic devices using passive control by externally driven flows that are varied locally by geometry of the channel in a continuous stream [2–6].

One of basic "unit operations" of droplet-based microfluidics is droplet generation [4] and breakup [5–9] in *T* junction geometry. Droplets of controllable size can be formed when two immiscible fluids enter the *T* junction through two inlet channels. On the other hand, confined droplets suspended in an immiscible carrier liquid break up into two smaller droplets of highly controllable size as they enter the *T* junction through the inlet channel; following the breakup each of the two daughter droplets move through the two outlet channels. The two modes of droplet breakup have been identified in experiments [7]: the breakup "with tunnels" and "obstructed" breakup regime (see Fig. 1). The former regime is operative for relatively short droplet whereas its critical quasistatic "dumbbell" shape was suggested to be controlled by an elevated upstream pressure due to lubricating flow through the "tunnels" formed between the droplet and the outlet channel walls [8]. Beyond the critical elongation a fast central pinch off occurs due to capillary instability [5]. The theory proposed in [8] was found to be in a good agreement with experimental findings [7] and results of numerical simulations [9].

In the "obstructed" regime, however, the slender droplet blocks the outlet channels for all times, so that the breakup is intrinsically transient (see Fig. 1) and it has not been addressed in details until now. Following same arguments as in [8], we start with a simple 2D geometric construction for the interface shape in the depression region (see Fig. 2 for the notation). We assume that for surface tension dominated flow, the depression region can be well approximated by a circular arc with a radius $R(t)$ (supported by experimental observations [7] and our numerical simulations). The vertical position z of the droplet concave surface is defined by the equation $z(\varphi) = \delta + R(1 - \cos\varphi)$, where δ is the "neck" width, and φ is the angle measured from the (vertical) symmetry axis. The arc shape is joined (sharply) with a horizontal line at $z = w$, where w is the channel width, corresponding to an angle φ_0 so that $x' = R\sin\varphi_0$. In fact, the interface shape is smooth at the smaller length scale defined by the thickness of the film sandwiched between the wall and the squeezing droplet, we will discuss this later. The neck width in terms of R and φ_0 is given by $\delta = w - R(1 - \cos\varphi_0)$ and the volume of the depression region occupied by the carrier liquid reads, $V_d = R^2(\varphi_0 - \frac{1}{2}\sin 2\varphi_0)$.

Mass conservation further dictates that the rate-of-change of the displaced volume is equal to the inlet flow rate $\dot{V}_d = \mathcal{F}(\dot{R}, \dot{\varphi}_0, R, \varphi_0) = Uw$, where U is the mean

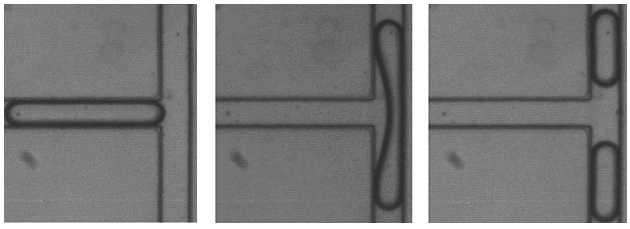

FIG. 1. The "obstructed" breakup regime observed in experiments [7] using fluorinated oil droplet in water; the time progresses from left to right. The scales are the same for all figures with 80 μm high and 80 μm wide microchannels.

 © 2012 American Physical Society

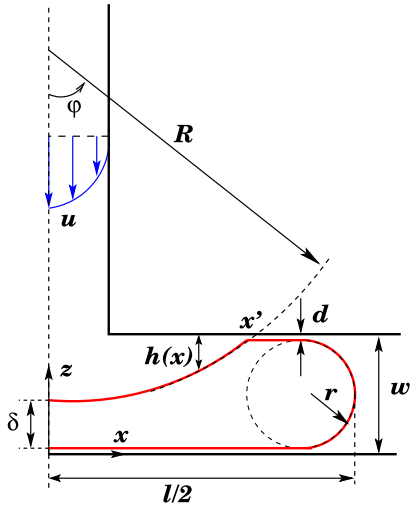

FIG. 2 (color online). Schematic of the geometric construction for the transient droplet shape; l stands for the deformed droplet length, w is the width of the channel, R is the curvature radius of the depression region, φ is the polar angle counted from the symmetry axis, d is the lubricating film thickness, $r \approx w/2$ is the curvature of the advancing meniscus, and δ is the width of the "neck."

inlet velocity and the dot stands for time derivative. In the vicinity of the edge, x', (see Fig. 2) where the capillary forces balance the viscous forces due to the externally imposed flow, we assume that at x' the Tanner's law [10] for the local contact angle applies, i.e., $\varphi_0^3 \sim U'\mu/\gamma$, where γ is the constant interfacial tension, μ is the dynamic viscosity of the carrier liquid and $U' = dx'/dt$ is the edge velocity [11]. Therefore, we have $\dot{x}' = \frac{d}{dt}(R\sin\varphi_0) = \alpha\frac{\gamma}{3\mu}\varphi_0^3$ where α is a universal constant. Scaling the length with w and time with w/U we obtain a system of two coupled ordinary differential equations (ODE) governing the evolution of the dimensionless depression volume $\hat{V}_d \approx 2\hat{R}^2\varphi_0^3/3$ and the edge position $\hat{x}' = \hat{R}\varphi_0$ with time τ

$$\frac{d}{d\tau}\left(\frac{2}{3}\hat{R}^2\varphi_0^3\right) \approx 1, \qquad \frac{d}{d\tau}(\hat{R}\varphi_0) \approx \left(\frac{\alpha}{3\mathrm{Ca}}\right)\varphi_0^3, \quad (1)$$

where $\mathrm{Ca} = U\mu/\gamma$ is the capillary number. Since Eqs. (1) involve only powers of $\hat{R}$ and φ_0, after a short initial transient the solution follows a power-law dependence $\hat{R}(\tau) \sim \tau^a$ and $\varphi_0(\tau) \sim \tau^b$. Substituting these into (1) we readily obtain the exponents,

$$\hat{R} \approx \mathcal{A}\left(\frac{\alpha}{3\mathrm{Ca}}\right)^{3/7}\tau^{5/7}, \quad \varphi_0 \approx \mathcal{B}\left(\frac{\alpha}{3\mathrm{Ca}}\right)^{-2/7}\tau^{-1/7}, \quad (2)$$

where the preexponential factors $\mathcal{A} = 3^{2/7}7^{3/7}/2^{8/7} \simeq 1.427$ and $\mathcal{B} = 2^{3/7}3^{1/7}/7^{2/7} \simeq 0.903$. The dynamics of the neck thinning $\hat{\delta}(\tau) = \delta/w$ and the edge displacement, $\hat{x}'(\tau) = x'/w$, can be readily found from (2) as

$$\hat{x}' \approx \hat{R}\varphi_0 \simeq 1.289\left(\frac{\alpha}{3\mathrm{Ca}}\right)^{1/7}\tau^{4/7}, \quad (3)$$

$$\hat{\delta} \approx 1 - \frac{1}{2}\hat{R}\varphi_0^2 \simeq 1\text{–}0.582\left(\frac{\alpha}{3\mathrm{Ca}}\right)^{-1/7}\tau^{3/7}. \quad (4)$$

The asymptotic results provide a qualitative support for the experimental findings in [7] showing a very weak dependence of $\hat{\delta}(\tau)$ and $\hat{x}'(\tau)$ on Ca.

To ascertain the predictions of our theory, we conducted direct numerical simulations of "obstructed" breakup of 2D droplet using an in-house code based on a volume of fluid (VoF) approach combined with "height function" (HF) methodology for accurate computation of interfacial normal and curvature. Using the HF methodology and a consistent formulation of surface tension forces, we have extended the applicability of our VoF method for modeling such low-Ca phenomena. The details of the numerical discretization and code validations are provided in [9,13]. We use an adaptive mesh refinement [14] to focus the computations on the regions of importance such as where the velocity gradient is high or the film between the droplet and the channel wall; Fig. 3(a) depicts a typical adaptive mesh utilized for the numerical simulations along with the droplet shape and the pressure distribution shown in the background. The no-slip boundary condition is applied at the walls of the channel; at the inlet, a uniform normal velocity, U, is applied with a zero gradient condition for

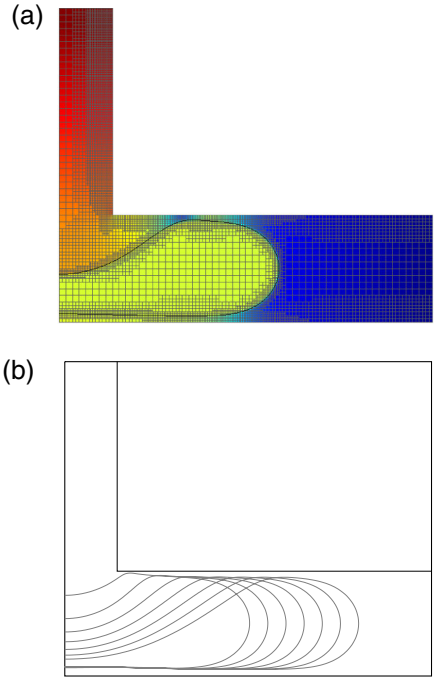

FIG. 3 (color online). (a) Snapshot of adaptive numerical mesh along with the droplet shape and pressure distribution (color map) for $\mathrm{Ca} = 0.06$ and $l_0/w = 3.25$; (b) Snapshots of numerically computed droplet profiles, $\mathrm{Ca} = 0.08$ and $l_0/w = 3.25$.

the pressure. At the outlet, a typical outflow boundary condition, zero pressure and velocity gradient, are applied. Figure 3(b) shows the snapshots of the computed droplet profiles at different times during the "obstructed" breakup.

The comparison of the results of numerical simulations and the theoretical predictions is shown in Figs. 4(a) and 4(c). The constant α is found from fitting (3) and (4) to the results of numerical simulations yielding $\alpha \simeq 0.25$. The numerical results are recast according to Eqs. (3) and (4); i.e., the edge position $(x'/w)(\alpha/3\mathrm{Ca})^{-1/7}$ and the scaled depression depth $(1-\delta/w)(\alpha/3\mathrm{Ca})^{1/7}$ are depicted vs $\tau = Ut/w$ in log-log coordinates in Figs. 4(a) and 4(b), respectively. In the first case, all the data corresponding to various Ca's collapse on the master curve $1.29\tau^{4/7}$, while in the latter case the numerical results conform to $0.69\tau^{3/7}$. The inset in Fig. 4(a) shows the edge position x'/w vs Ut/w in experiments [7] for Ca in the range $6\times10^{-4} - 2.8\times10^{-3}$; it can be readily seen that the data conform well to the 4/7 scaling (3). The depression region in the numerical simulations [as in Fig. 3(b)] is approximated by a circular arc and the resulting radius of curvature is rescaled according to (2) as $(R/w)(\alpha/3\mathrm{Ca})^{-3/7}$ and plotted vs time τ in Fig. 4(c); there is an excellent agreement between the numerical results and the theoretical prediction (2) both in terms of scaling with Ca and time, as the numerical data falls on the master curve $1.43\tau^{5/7}$.

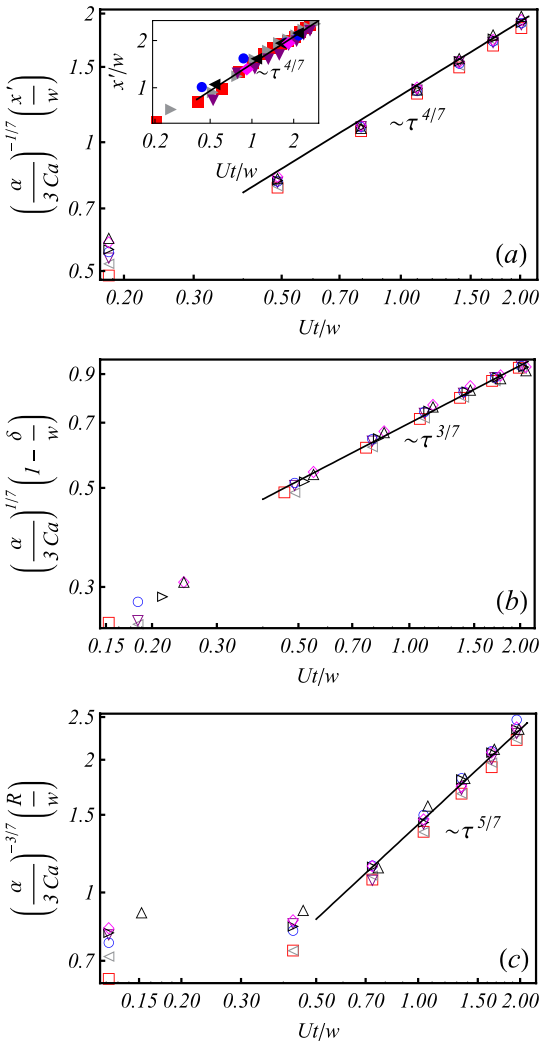

FIG. 4 (color online). Comparison of the numerical results (void symbols) vs the theoretical predictions in Eqs. (2)–(4) (solid lines) with $\alpha = 0.25$ in log-log coordinates for Ca = 0.02 (□), Ca = 0.03 (◁), Ca = 0.04 (▽), Ca = 0.05 (○), Ca = 0.06 (▷), Ca = 0.08 (◇), and Ca = 0.1 (△). (a) the edge position $(x'/w)(\alpha/3\mathrm{Ca})^{-1/7}$, plotted vs time $\tau = Ut/w$; inset shows the experimental results x'/w vs Ut/w (full symbols) for Ca in the range between $6\times10^{-4} - 2.8\times10^{-3}$ [7]; (b) scaled depression width $(1-\delta/w)(\alpha/3\mathrm{Ca})^{1/7}$ vs time $\tau = Ut/w$; (c) extrapolated curvature radius of the depression region $(R/w)(\alpha/3\mathrm{Ca})^{-3/7}$.

The similarity solution can be readily used to determine the boundary between the obstructed and nonobstructed breakup in plane of parameters $(l_0/w, \mathrm{Ca})$, where l_0 is the initial length of the confined droplet in the inlet channel. Neglecting the volume confined in the lubricating films sandwiched between the droplet and the channel wall, the initial volume of the droplet reads $V_0 \approx (l_0 - w)w + \pi w^2/4$. As the position of the depression edge, x', reaches the leading tip of the droplet, volume conservation implies $V_0 = 2x'w + \pi w^2/4 - V_d$. Substituting the previous expression for V_0 we arrive at $\hat{l}_0 = 2\hat{x}' - \hat{V}_d + 1$, where $\hat{l}_0 = l_0/w$ and $\hat{V}_d = V_d/w^2$. The "obstructed" breakup occurs when the neck thins out before the "tunnels" opens, i.e., before the leading edge of the depression region reaches the droplet leading edge. Therefore the boundary separating obstructed and nonobstructed breakup can be determined from the above expression for $\hat{l}_0$ with $\hat{x}'_*$ and $\hat{V}_{d*}$ corresponding to a time when the neck thins out, i.e., $\hat{\delta} = 0$. This time can be found from (4) as $\tau_* \approx 3.54(\alpha/3\mathrm{Ca})^{1/3}$. Using (2), we find that after time τ_*, the position of the edge will be $\hat{x}'_* \approx \hat{R}_*\varphi_* \approx 2.65(\alpha/3\mathrm{Ca})^{1/3}$ and $\hat{V}_{d*} = \tau_* \approx 3.54(\alpha/3\mathrm{Ca})^{1/3}$. Using these we obtain the expression for the threshold for the onset of the obstructed breakup:

$$\frac{l_0}{w} = 1.76\left(\frac{\alpha}{3\mathrm{Ca}}\right)^{1/3} + 1. \tag{5}$$

The stability diagram based on the numerical results is depicted in Fig. 5 (solid line) for $\alpha = 0.25$ showing an excellent agreement between the theory and the results of VoF-HF numerical simulations.

Under the assumption of small Ca, the analysis of the flow admits a standard lubrication evolution equation for the gap thickness $h(x, t)$ as a function of the stream-wise distance x and time (see Fig. 2):

$$h_t + \frac{\gamma}{3\mu}(h^3 h_{xxx})_x = 0. \tag{6}$$

For the constant inlet flow velocity U, the analysis of the steady motion of the front edge in the form $h(x - Ut/2)$ is

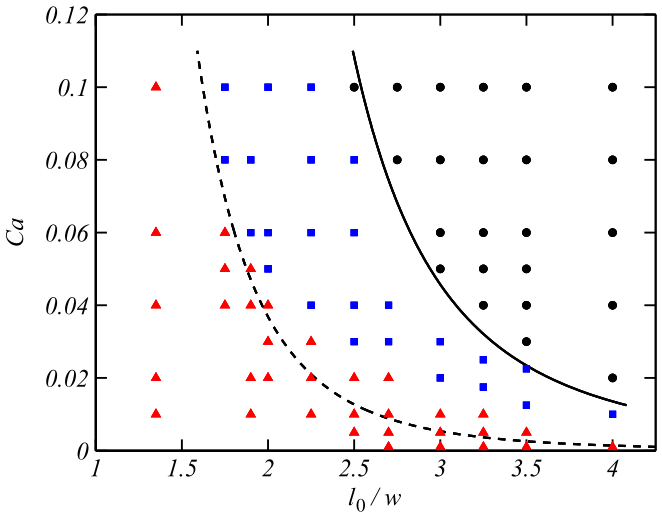

FIG. 5 (color online). Phase diagram of numerical simulations for a drop in a symmetric T junction. The dashed line $l_0/w = 0.98\mathrm{Ca}^{0.21}$ [8] marks the boundary between breaking and nonbreaking drops; the solid line corresponds to Eq. (5) with $\alpha = 0.25$ and it separates obstructed and nonobstructed breakup regimes. Symbols correspond to numerical results for nonbreaking (▲), breaking drops without obstruction (■), and breaking drops with obstruction (●).

identical to that in [12], whereas (6) transforms into a standard Landau-Levich-Bretherton (LLB) equation $\eta_{\xi\xi\xi} = (\eta - 1)/\eta^3$, where the variables are rescaled as $h = d\eta$ and $x = d(3/2\mathrm{Ca})^{-1/3}\xi$, resulting in lubricating film thickness $d \sim w\mathrm{Ca}^{2/3}$ and the velocity of the meniscus in the outlet channel equal to $U(1/2 + \mathcal{O}(\mathrm{Ca}^{2/3}))$ as confirmed by our VoF-HF simulations.

The dynamics of the depression region considered earlier in an approximate fashion can now be resolved in terms of self-similar solution of (6). Using the initial depth of the depression, h_0, and $3\mu h_0/\gamma$ as the characteristic length and time, respectively, we arrive at the equation for the scaled depression depth H:

$$\partial_\tau H + \partial_\xi(H^3 H_{\xi\xi\xi}) = 0. \tag{7}$$

We further look for the similarity solution in the form $H(\xi, \tau) = \tau^{-a}\mathcal{H}(\xi/\tau^b)$. Substituting this ansatz into (7), we find that the ODE for $\mathcal{H}(\zeta)$, where $\zeta = \xi/\tau^b$ denotes the similarity variable, is only derived when $a = (1 - 4b)/3$. Since the depression volume grows linearly with time, $\int H d\xi = \int \tau^{-a}\mathcal{H}(\xi/\tau^b)d\xi \sim \tau$, it implies that $a = b - 1$ yielding $b = 4/7$ and $a = -3/7$. Thus, the depression depth grows $\sim\tau^{3/7}$ while it extends as $\sim\tau^{4/7}$. This is in a complete agreement with the exponents obtained from the approximate solution (3) and (4). Note that the requirement of fixed volume, $\int H d\xi = \text{const}$, results in well-known exponents $a = b = 1/7$ corresponding to spreading of a cylindrical droplet [10]. Substituting $H = \tau^{3/7}\mathcal{H}(\xi/\tau^{4/7})$ into (7) gives

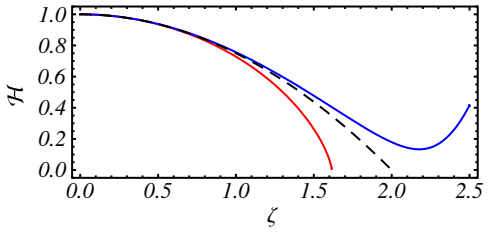

FIG. 6 (color online). Numerical solution of Eq. (8) for $\mathcal{H}(0) = 1$ and $\mathcal{H}''(0) = -0.5$ [lower (red) curve]. The solution vanishes at $\zeta_* \simeq 1.616$. The dashed curve is the asymptotic "circular cap" solution for the center of the drop $\mathcal{H} \sim 1–0.5\zeta^2/2$. The similarity solution for spreading of the cylindrical droplet with fixed volume is provided for comparison [upper (blue) curve].

$$(\mathcal{H}^3\mathcal{H}''')' - \frac{4}{7}\zeta\mathcal{H}' + \frac{3}{7}\mathcal{H} = 0, \tag{8}$$

where prime stands for the derivative with respect to the similarity variable $\zeta = \xi/\tau^{4/7}$. We numerically integrate this equation setting $\mathcal{H}(0) = c_0$ and $\mathcal{H}''(0) = -c_2$ and the result of the integration for $c_0 = 1$ and $c_2 = -0.5$ are depicted in Fig. 6 [lower (red) curve]. In the central part of the depression region, $\mathcal{H}''' \approx 0$, yielding a "circular cap" solution $\mathcal{H} \sim c_0 - \frac{c_2}{2}\zeta^2$ (dashed line in Fig. 6). Note that $\mathcal{H}(\zeta)$ vanishes at some finite value of ζ [15] while we look for solutions that tend to a constant thickness $d \sim w\mathrm{Ca}^{2/3}$. The similarity ("outer") solution of (8) should then be matched with the ("inner") solution of LLB-type equation describing dynamics of the droplet edge on a length scale of the film thickness d. The matching procedure should be similar to that developed for spreading drop in the presence of an interface potential [16] and is beyond the scope of the present Letter.

We would like to thank Len Pismen for fruitful discussions. A. M. L. acknowledges the support of the Israel Science Foundation (ISF) via the Grant No. 1319/09 and Joliot Chair visiting position at Ecole Supérieure de Physique et Chimie de Paris (ESPCI). S. A. acknowledges the use of XSEDE through TG-DMS110019 for computational resources. M.-C. J. and P. T. acknowledge CNRS and ESPCI for their support.

*lisha@technion.ac.il

[1] H. A. Stone, A. D. Stroock, and A. Ajdari, Annu. Rev. Fluid Mech. **36**, 381 (2004); R. Seeman, M. Brinkmann, T. Pfohl, and S. Herminghaus, Rep. Prog. Phys. **75**, 016601 (2012).
[2] S. Sugiura, M. Nakajima, S. Iwamoto, and M. Seki, Langmuir **17**, 5562 (2001).
[3] P. B. Umbanhowar, V. Prasad, and D. A. Weitz, Langmuir **16**, 347 (2000).
[4] T. Thorsen, R. W. Roberts, F. H. Arnold, and S. R. Quake, Phys. Rev. Lett. **86**, 4163 (2001); J. D. Tice, H. Song, A. D.

Lyon, and R. F. Ismagilov, Langmuir **19**, 9127 (2003); P. Garstecki, M. J. Fuerstman, H. A. Stone, and G. M. Whitesides, Lab Chip **6**, 437 (2006); B. Dollet W. van Hoeve, J.-P. Raven, P. Marmottant, and M. Versluis, Phys. Rev. Lett. **100**, 034504 (2008); V. van Steijn, C. R. Kleijn, and M. T. Kreutzer, Phys. Rev. Lett. **103**, 214501 (2009).

[5] D. R. Link, S. L. Anna, D. A. Weitz, and H. A. Stone, Phys. Rev. Lett. **92**, 054503 (2004).

[6] Y. C. Tan, J. S. Fisher, A. I. Lee, V. Cristini, and A. P. Lee, Lab Chip **4**, 292 (2004).

[7] M.-C. Jullien, M.-J. Tsang Mui Ching, C. Cohen, L. Menetrier, and P. Tabeling, Phys. Fluids **21**, 072001 (2009).

[8] A. M. Leshansky and L. M. Pismen, Phys. Fluids **21**, 023303 (2009).

[9] S. Afkhami, A. M. Leshansky, and Y. Renardy, Phys. Fluids **23**, 022002 (2011).

[10] L. Tanner, J. Phys. D **12**, 1473 (1979); P.-G. de Gennes, Rev. Mod. Phys. **57**, 827 (1985).

[11] In the present case liquid edge advances over the preexisting film of thickness $d \sim w\mathrm{Ca}^{2/3}$ controlled by the dynamics of meniscus in the outlet channel [12].

[12] F. P. Bretherton, J. Fluid Mech. **10**, 166 (1961).

[13] S. Afkhami and M. Bussmann, Int. J. Numer. Methods Fluids **57**, 453 (2008).

[14] S. Popinet, J. Comput. Phys. **190**, 572 (2003).

[15] Interestingly, the similarity equation, $\mathcal{H}^2\mathcal{H}''' = \zeta/7$, corresponding to capillary spreading of the cylindrical droplet with a fixed volume, does not posses solutions for which $\mathcal{H}(\zeta)$ goes to zero at a finite value of $\zeta = \xi/\tau^{1/7}$ [upper (blue) curve in Fig. 6].

[16] L. M. Pismen and J. Eggers, Phys. Rev. E **78**, 056304 (2008).